AFRL-RX-WP-TR-2009-4167

PHOTONIC CRYSTALS FOR INFRARED NONLINEAR OPTICS

Yoel Fink, Marin Soljacic, Peter T. Rakich, Ayman Abouraddy, Zachary Ruff, and Ofer Shopira

Massachusetts Institute of Technology

FEBRUARY 2009
Final Report

AIR FORCE RESEARCH LABORATORY
MATERIALS AND MANUFACTURING DIRECTORATE
WRIGHT-PATTERSON AIR FORCE BASE, OH 45433-7750
AIR FORCE MATERIEL COMMAND
UNITED STATES AIR FORCE

NOTICE AND SIGNATURE PAGE

Using Government drawings, specifications, or other data included in this document for any purpose other than Government procurement does not in any way obligate the U.S. Government. The fact that the Government formulated or supplied the drawings, specifications, or other data does not license the holder or any other person or corporation; or convey any rights or permission to manufacture, use, or sell any patented invention that may relate to them.

This report was cleared for public release by the USAF 88th Air Base Wing (88 ABW) Public Affairs Office (PAO) and is available to the general public, including foreign nationals. Copies may be obtained from the Defense Technical Information Center (DTIC) (http://www.dtic.mil).

AFRL-RX-WP-TR-2009-4167 HAS BEEN REVIEWED AND IS APPROVED FOR PUBLICATION IN ACCORDANCE WITH THE ASSIGNED DISTRIBUTION STATEMENT.

*//Signature//

JONATHAN GOLDSTEIN
Work Unit Manager
Electronic and Optical Materials Branch
Survivability and Sensor Materials Division

//Signature//

JOSEPH A. BAKER, Chief
Electronic and Optical Materials Branch
Survivability and Sensor Materials Division

//Signature//

KRISTINE L. TITTLE, Division Deputy
Composite and Hybrid Materials Branch
Nonmetallic Materials Division
Materials and Manufacturing Directorate

This report is published in the interest of scientific and technical information exchange, and its publication does not constitute the Government's approval or disapproval of its ideas or findings.

*Disseminated copies will show "//Signature//" stamped or typed above the signature blocks.

REPORT DOCUMENTATION PAGE

Form Approved
OMB No. 0704-0188

1. REPORT DATE *(DD-MM-YY)*	2. REPORT TYPE	3. DATES COVERED *(From - To)*
February 2009	Final	01 May 2005 – 13 February 2009

4. TITLE AND SUBTITLE
PHOTONIC CRYSTALS FOR INFRARED NONLINEAR OPTICS

5a. CONTRACT NUMBER
FA8650-05-C-5426

5b. GRANT NUMBER

5c. PROGRAM ELEMENT NUMBER
62102F

6. AUTHOR(S)
Yoel Fink, Marin Soljacic, Peter T. Rakich, Ayman Abouraddy, Zachary Ruff, and Ofer Shopira

5d. PROJECT NUMBER
4348

5e. TASK NUMBER
73

5f. WORK UNIT NUMBER
73100012

7. PERFORMING ORGANIZATION NAME(S) AND ADDRESS(ES)
Massachusetts Institute of Technology

8. PERFORMING ORGANIZATION REPORT NUMBER

9. SPONSORING/MONITORING AGENCY NAME(S) AND ADDRESS(ES)
Air Force Research Laboratory
Materials and Manufacturing Directorate
Wright-Patterson Air Force Base, OH 45433-7750
Air Force Materiel Command
United States Air Force

10. SPONSORING/MONITORING AGENCY ACRONYM(S)
AFRL/RXPS

11. SPONSORING/MONITORING AGENCY REPORT NUMBER(S)
AFRL-RX-WP-TR-2009-4167

12. DISTRIBUTION/AVAILABILITY STATEMENT
Approved for public release; distribution unlimited.

13. SUPPLEMENTARY NOTES
PAO Case Number: 88ABW-2009-1185; Clearance Date: 25 Mar 2009. Report contains color.

14. ABSTRACT
Here we summarize our progress in the development of 2- to 5-micron wavelength supercontinuum sources through grant number FA8650-05-C-5426 over the life of the program. The key developments over the past 3 years include l) A proof-of-principle demonstration of a novel, efficient mid-IR Raman laser source in silica materials system, yielding efficient spectral transfer to 2.41 microns. (The demonstrated system can be naturally extended in wavelength to 5microns and beyond); 2) The development of nonlinear-optical simulation capabilities; 3) Progress toward the development of low loss, highly nonlinear chalcogenide fibers; 4) Novel interferometric measurement techniques to examine the integrity and loss mechanisms of such fibers; and 5) Nonlinear studies of chalcogenide fibers and prospects for extending our cascaded Raman source to longer wavelengths.

15. SUBJECT TERMS
infrared fiber, supercontinuum, Raman-shifting, cha1cogenide, photonic band gap

16. SECURITY CLASSIFICATION OF:			17. LIMITATION OF ABSTRACT:	18. NUMBER OF PAGES	19a. NAME OF RESPONSIBLE PERSON (Monitor)
a. REPORT	b. ABSTRACT	c. THIS PAGE			Jonathan Goldstein
Unclassified	Unclassified	Unclassified	SAR	38	19b. TELEPHONE NUMBER *(Include Area Code)* N/A

Standard Form 298 (Rev. 8-98)
Prescribed by ANSI Std. Z39-18

Introduction

The goal of this program was to develop a multi-watt mid-IR laser source spanning the 2-5 micron wavelength range with a multi-watt output. The primary challenges faced in meeting these goals were: (1) to develop novel multi-material chalcogenide optical fibers to facilitate nonlinear spectral generation over the 2-5 micron wavelength range, (2) to engineer and validate a novel laser source (based on nonlinear processes) which could enable the generation of 2-5 micron wavelengths within such chalcogenide materials systems, (3) implement the novel laser source concept using chalcogenide fibers and scale to high powers.

Through the life of this program, we will show that we have made tremendous strides in the development small-core, highly-nonlinear chalcogenide fibers in hybrid chalcogenide and polymer materials systems, and we were successful in developing and demonstrating a novel type of cascaded Raman laser which operates optimally in normal dispersion (a critical requirement for efficient spectral generation in chalcogenide fibers). Through validation of our new laser concept we demonstrated highly efficient transfer of power from 1.5 microns to 2.41 microns in normal dispersion silica fibers. Furthermore, we have performed extensive nonlinear studies on our newly developed chalcogenide fibers at both nanosecond and femtosceond timescales, demonstrating spectral generation through both stimulated Raman spectral generation and self-phase modulation. However, due to the complicated nature of chalcogenide materials system, further work is required before we can meet the challenging goals of the program. Currently there are two primary challenges that require further work: (1) Further work must be done to understand the various mechanisms for damage of chalcogenide fibers. (2) Further work is required to reduce the losses of our fibers and improve the purity of the chalcogenide materials used. Through nonlinear studies, we have found that optically induced damage to the fibers was observed at a wide range of powers (often much lower that expected), indicating that we are not currently limited by the fundamental material damage thresholds. Currently, laser-induced damage and the limited interaction lengths achieved through our fibers limit our ability to extend the spectral output of our laser system using our newly developed chalcogenide fibers.

Section 1 –Nonlinear source development

The primary challenges of developing long wavelengths sources through nonlinear processes in chalcogenide fibers is due to the fact that chalcogenide glasses possess a very large normal material dispersion. Furthermore, chalcogenide materials are known to have relatively low damage thresholds, meaning that the peak powers produced within the material must be limited. Unfortunately, anomalous dispersion is required to produce conventional supercontinuum based spectra through soliton effects and modulation instabilities. While one could imagine shrinking the core-size of an optical fiber to sub-micron dimensions in order to flip the sign of the total chromatic dispersion from normal to anomalous, due to the low damage threshold of such materials, this wouldn't be a feasible solution for the generation of high average laser output powers. Therefore, through this research, we sought to identify and exploit nonlinear processes which could be effective for long wavelength spectral generation in the presence of normal chromatic dispersion.

In this section, we show through both simulation and experiment that cascaded Raman amplification is the most practical and effective means of long wavelength spectral generation in the presence of normal chromatic dispersion. Furthermore, it can be seen that since this nonlinear process does not produce large variations in the peak pulse intensity (as is a problem in the case of modulation instability and soliton effects) this process is ideal for use in chalcogenide fibers, which are susceptible to damage at low peak powers.

Unfortunately, virtually no work has been done to develop and perfect cascaded Raman amplification for the purpose of mid-IR spectral generation (which we believe to be ideal for use in chalcogenide fibers). Therefore, before implementing this approach to long wavelength spectral generation in more complicated chalcogenide materials systems, we first study and validate our proposed long wavelength laser concept using silica fibers which possess normal chromatic dispersion (similar to chalcogenide materials). The key questions that we pose through the study of this process are: (1) what are the limitations to generating long wavelengths through cascaded Raman amplification? (2) How can we best engineer the dispersion and nonlinearity to maximize the efficiency of the spectral red-shift produced through cascaded Raman amplification?

1.1 Basics of the cascaded Raman process

At high peak powers, it is known that Raman amplification can result in efficient spectral red-shifts of incident laser-light from the pump to Stokes wavelengths (seen in Fig. 1). Raman gain has been widely studied in silica fibers, yielding a spontaneously generated stokes shift of $\Omega \sim 14.7$ THz. For increasing peak powers and nonlinear interaction lengths, it has also been demonstrated that these spectral red shifts can be made to occur several times over. For instance, through fourth order cascaded Raman amplification, an experimental example of which is seen in Fig. 2 (taken from Lin, Cohen, IEEE JQE, 14 (11), 855 1978), the incident laser frequency (ω_p) is stokes shifted four times yielding spectral power at $\omega_p - \Omega$, $\omega_p - 2\Omega$, $\omega_p - 3\Omega$, $\omega_p - 4\Omega$. Through experimental study of silica, we seek to optimize the cascaded Raman process for the production of efficient generation of mid-IR wavelengths.

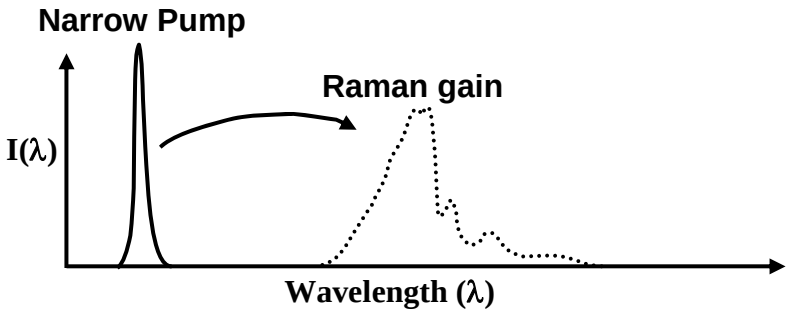

Figure 1 Illustration showing the silica Raman gain produced by a bright incident laser.

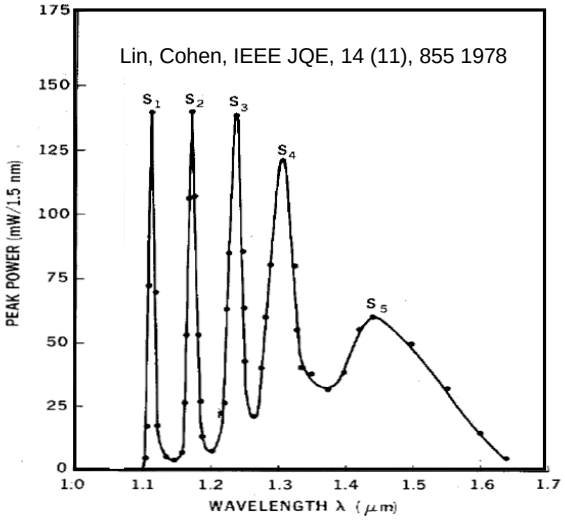

Figure 2. Example of cascaded Raman amplification in silica fibers using an Nd:YAG laser source. S1 is the incident pump while S2-S5 are generated Stokes orders.

Upon examination of the experimental data obtained by Lin and Cohen in 1978 (seen in Fig. 2), we note that through generation of each successive stokes order, the Raman spectrum significantly broadens. Due to the dependence of the Raman gain profile on the spectral width of the pump, this spectral broadening significantly limits the generation of each successive stokes order. Therefore, to optimize the efficiency and maximum possible red-shift via this process, we seek to identify the cause of spectral broadening, and reduce its impact.

In principle there are two possible causes for the spectral broadening: (1) Spontaneous Raman emission and, (2) Four-wave mixing processes. Through exhaustive simulations, we have shown that four-wave mixing, in the form of modulation instability, is the primary source for the spectral broadening seen in Fig. 2. Unfortunately, some spectral broadening due to both spontaneous Raman emission and self-phase modulation are unavoidable in both normal and anomalous dispersion systems. However through the simulations shown in Fig. 3, it can be seen that the sign of the dispersion has a tremendous impact on the extent of the spectral broadening produced for a given amount of power. The simulations seen in Fig. 3 show the simulated temporal and spectral evolution of a nanosecond pulse with a peak power of 50 W in both normal (red curves) and anomalous (blue curves) fibers. Note, important to the realism of these simulations

was the inclusion of an amplified spontaneous emission, which tends to seed the modulation instability in experiments.

Upon examination, we see that after propagation through 80 meters of the anomalous fiber the spectrum has broadened from 0.01 nm 10 nm due to modulation instability, while after 80 meters of normal dispersion fiber, only a modest amount of self-phase modulation is seen. Furthermore, one can show that since the modulation instability is seeded by the amplified spontaneous emission (ASE), the degree of spectral broadening is also very sensitive to ASE. *Therefore, from these simulations, we conclude that in order to maximize the number of orders (i.e. to generate the most extreme spectral red-shift) we must minimize the ASE introduced to the system by the laser, and we seek a nonlinear fiber with normal chromatic dispersion.* Fortunately, since chalcogenide materials naturally exhibit a large normal chromatic dispersion, they appear to be ideally suited to optimize cascaded Raman amplification.

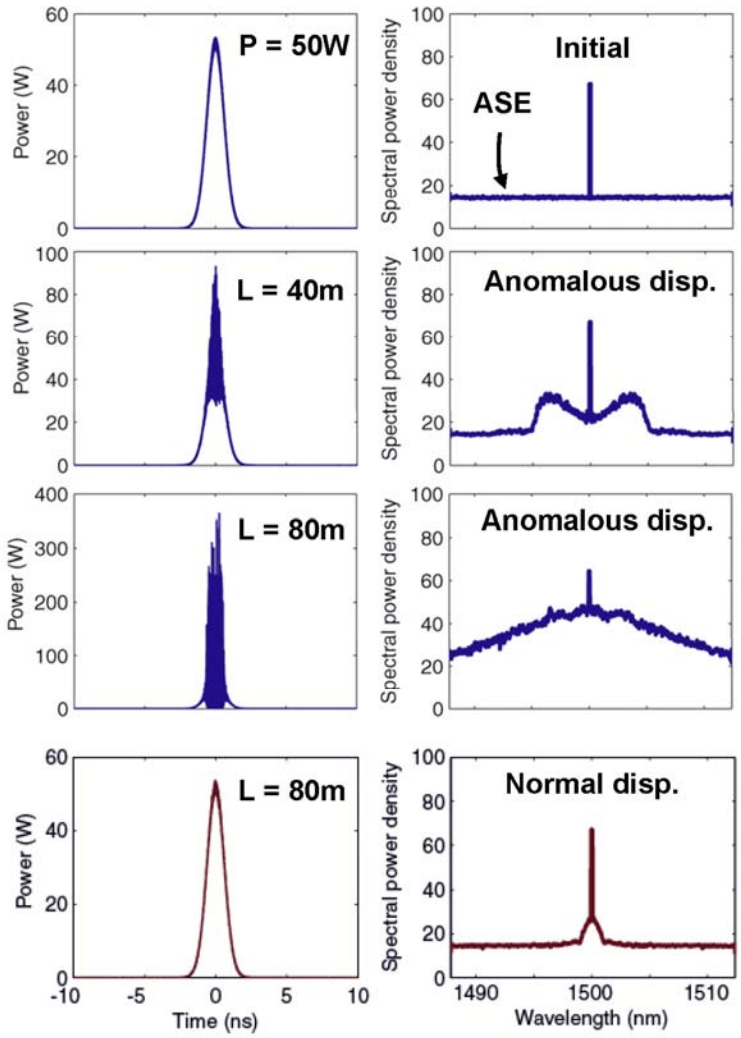

Figure 3. The Top panel shows the initial pulse and spectral profile simulated. The second and third panels show temporal and spectral evolution of the 1 ns pulse of Peak power 50W in 40 and 80 meters of silica fiber with anomalous dispersion (β_2 = -20 ps^2/km). The bottom panel shows temporal and spectral evolution of the 1 ns pulse of Peak power 50W in 80 meters silica fiber with normal dispersion (β_2 = +20 ps^2/km).

Through the first set of simulations discussed, we have examined the impact of four-wave mixing on the spectral orders produced through cascaded Raman amplification. However, the temporal evolution of the pulses through cascaded Raman amplification is also important to understanding what limits the efficiency of the cascaded Raman process. Figure 4 shows the temporal pulse evolution of a 1 nanosecond pulse through as it propagates through various distances along a normal dispersion fiber. The left panels show the shape of the pump pulse, while the right panels show the shape of the spontaneously generated stokes pulse. We see that through the transfer of power from the pump to stokes wavelengths, the center of the pulse is transferred leaving the wings of the pulse behind at the pump wavelength. From these simulations, we see that the highest power portion of the pulse is essentially preserved and transferred to the adjacent order, indicating that there are no fundamental barriers seen in the time domain to continuing this process for an arbitrarily large number of orders. It seems that the primary limitation is posed by the spectral broadening through each successive transfer of power.

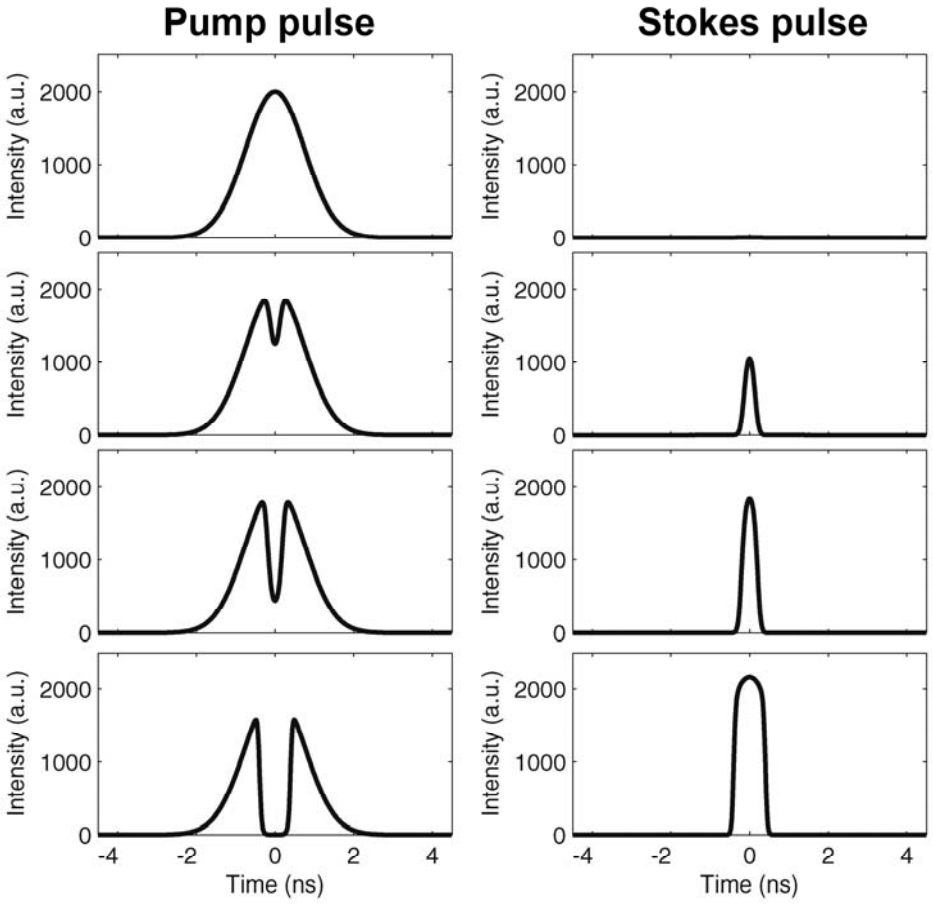

Figure 4. the temporal pulse evolution of a 1 nanosecond pulse through as it propagates through various distances along a normal dispersion fiber. The left panels show the shape of the pump pulse, while the right panels show the shape of the spontaneously generated stokes pulse.

1.2 Demonstration of Optimized Cascaded Raman for Mid-IR Spectral Generation

From previous simulations, we conclude that in order to maximize the number of orders (i.e. to generate the most extreme spectral red-shift) we must minimize the ASE introduced to the system by the laser, and we seek a nonlinear fiber with normal chromatic dispersion. For our first experimental test of this optimized cascaded Raman process, we seek to minimize complexity by performing our experiments in well known and robust silica materials systems.

Unfortunately, silica fibers generally possess anomalous dispersion from 1.3 to 2.4 μm owing to the presence of a strong mid-IR absorption resonance (as seen in Fig 5). However, normal fiber dispersion can be obtained over the entire silica transparency window through proper choice of fiber cutoff wavelength λc and NA. Since the waveguide dispersion of a step-index fiber is normal (in sign), and monotonically increasing in magnitude for wavelengths λc to 2.2λc, the waveguide dispersion can be made to match the material dispersion for sufficiently high NA, making the total chromatic dispersion of the fiber normal for all wavelengths. This can be seen in Fig. 5 which shows the dispersion for a silica step-index fiber with a cutoff wavelength of 1.45 μm and an NA of than 0.41, revealing that the zero dispersion wavelength is pushed to 2.6 μm, enabling normal dispersion for the entire transparency window of silica. A low OH content silica fiber with these parameters is produced by Nufern (Nufern UHNA7), the measured loss profile of which can be seen in Fig. 5.

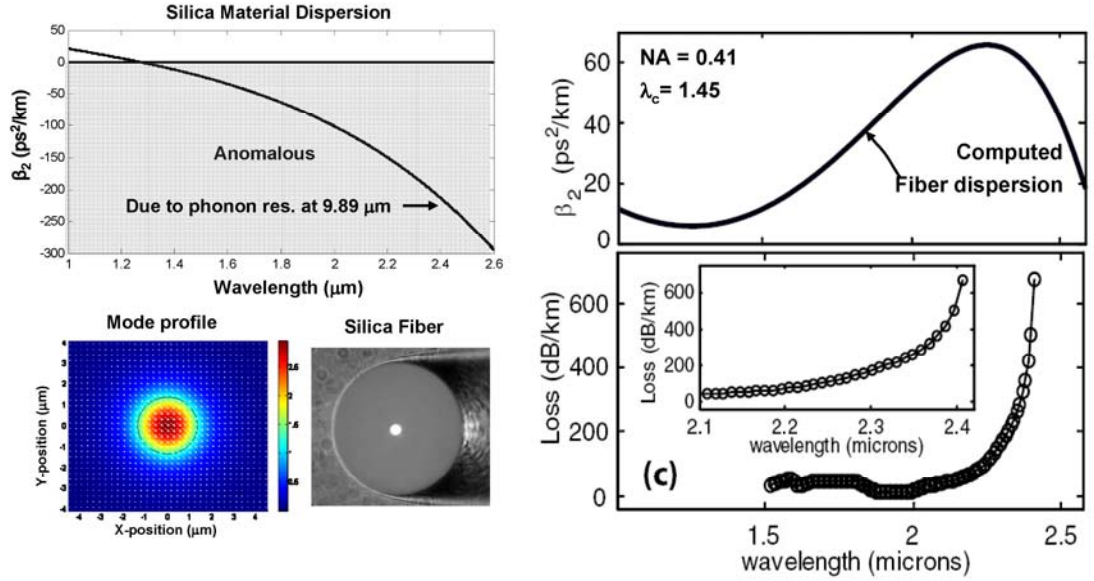

Figure 5: (Upper left) computed dispersion of bulk silica. (Lower Left) computed mode profile of Nufern step-index fiber. (Upper right) Computed chromatic dispersion of fiber including both material and waveguide dispersion. (Lower right) Measured loss of Nufern UHNA7 found through cutback method.

As discussed, Maximally efficient spontaneous Raman transfer requires a spectrally narrow laser source, with a low amplified spontaneous emission (ASE) pedestal, since the extent of FWM-induced spectral broadening is generally very sensitive to initial conditions. To this end, we developed the fiber-based laser source seen in Fig. 6,

which produces 2 ns pulses at a variable repetition rate, making output powers of several kilowatts possible. The source amplifies seed pulses from an electrically gain-modulated distributed-feedback (DFB) laser diode through two stages of erbium gain. In the first stage, the seed pulses of 1531.12 nm wavelength are co-propagated with a cw seed signal from a tunable laser source (detuned from the DFB wavelength by ~100 GHz). The cw signal produces saturation of the amplifiers, ensuring a very low ASE component to the amplified seed signal. Once the seed pulses reach 10 mW average power levels, a fiber Bragg grating with a 10-GHz-wide stopband is used, in conjunction with a circulator, to spectrally filter the seed pulses from the amplified cw laserline and ASE background signals. With sufficient power to saturate the second stage of erbium gain, the pulses are boosted to average powers of 240 mW, yielding an ASE component that is typically less than 1% of the total output power.

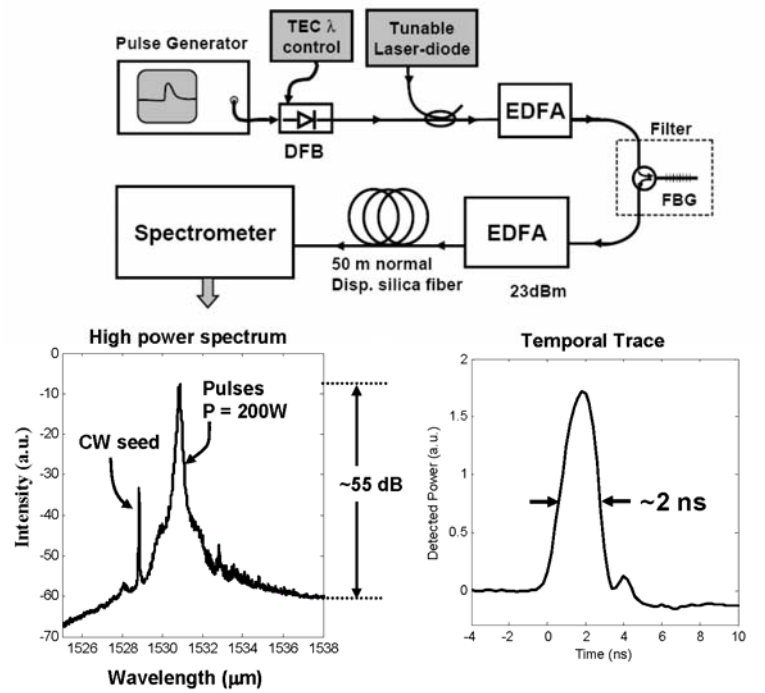

Figure 6. (Top) Schematic of laser source. (Lower left) Spectral output of laser. (Lower right) Temporal output of laser.

To produce spontaneous Raman energy transfer, the output of the high-power amplifier is spliced to 50 m of small-core normal-dispersion silica fibers (Nufern UHNA7). It should be noted that splice losses (0.5 dB) and linear propagation losses (1.5 dB). reduce the laser output power from 240 to 150 mW at 1.53 μm wavelengths. For a repetition rate of 680 kHz, the laser output is measured with spectrometer and PbSe detector as a function of laser power. The spectral evolution of the resulting cascaded Raman process is summarized by the spectral traces of Fig 7 and the intensity map of Fig. 8(a) as the laser power is increased, showing significant and controlled spectral red-shifts through higher-order CR power transfer. As the laser power is increased we see that the fundamental (1531 nms) pump wavelength is shifted in 14.7 THz (or 490 cm−1) steps to 1.64, 1.78, 1.94, 2.14, and 2.41 μm wavelength bands. While the spectral width of each successive order does broaden, the generated spectral bands are very clean,

showing negligible power shedding to continuum. Despite the high material losses of silica at 2.41 μm, a strong fifth Raman order is formed, producing significant power transfer.

The efficiency of power transfer to long wavelengths can be more precisely examined by integration of the laser power measured in each Raman order as the average laser power is increased. The measured fraction of laser power found in each order can be seen in Fig. 8(b), revealing that as much as 68% of the output power is transferred to the 2.14 μm wavelengths, while 30% is transferred to 2.41 μm wavelengths. Accounting for the splice and propagation losses of the fiber, we see that these percentages correspond to 37% and 16% total power conversion efficiencies to 2.14 μm and 2.41 μm wavelength bands, respectively. Remarkably, at maximum output power, less than 2% of the incident laser power remains at 1.53 μm.

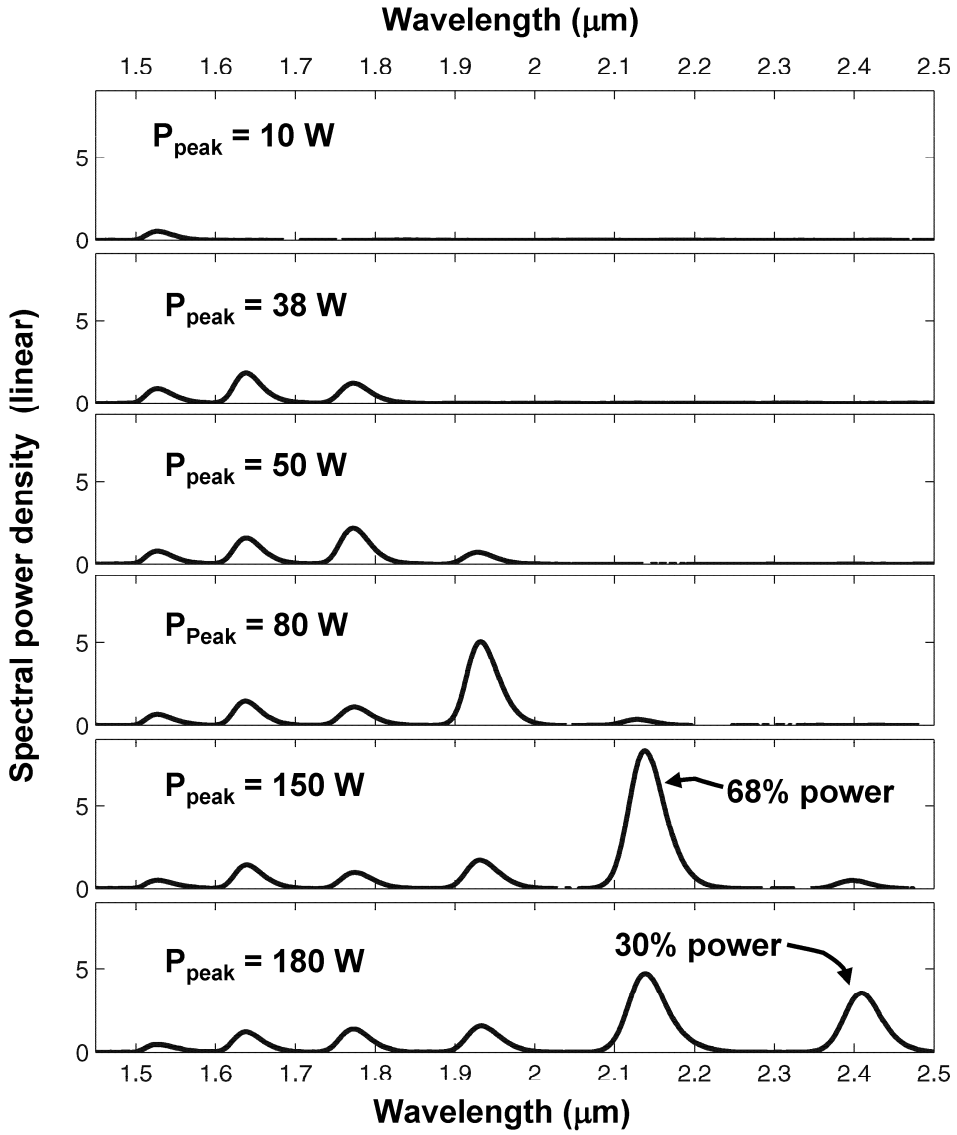

Figure 7. Measured Raman spectra from output of highly nonlinear silica fiber (Nufern UHNA 7) for increasing peak laser powers.

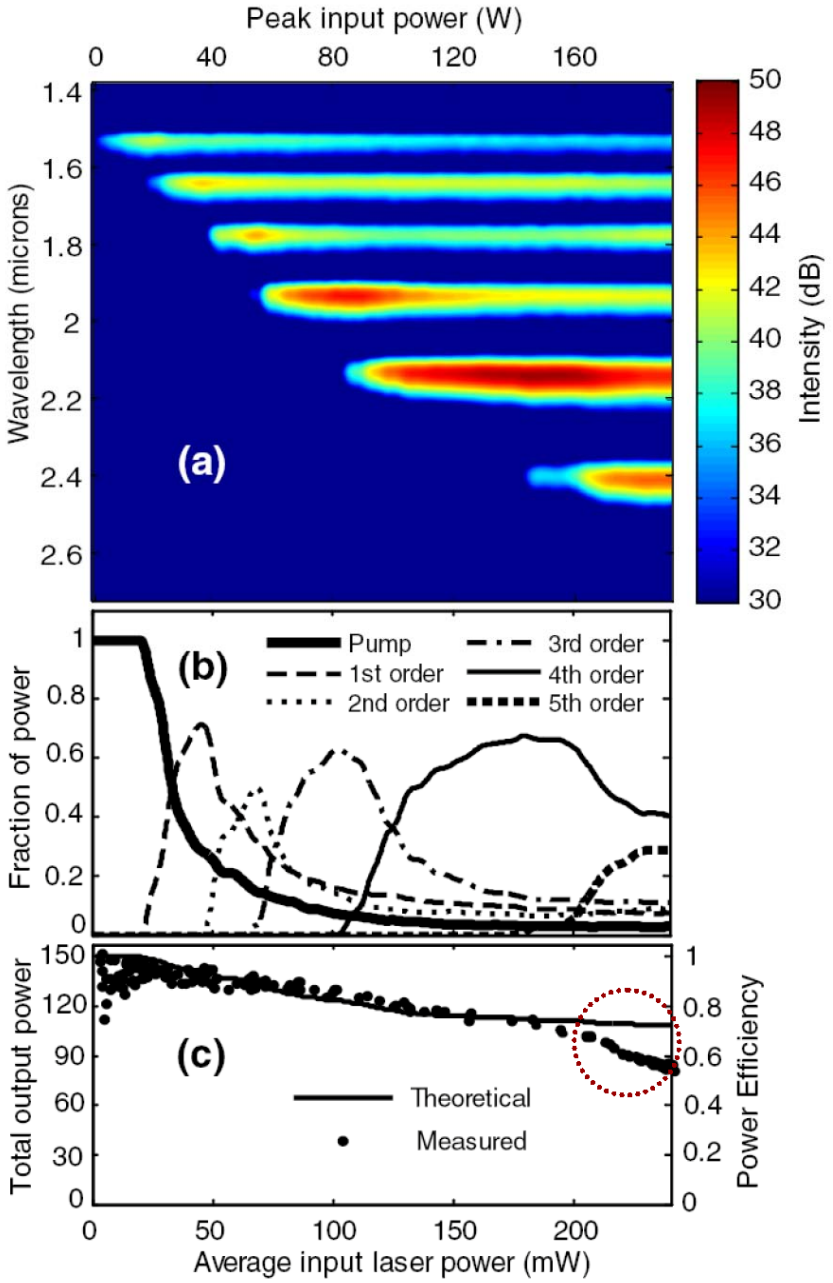

Figure 8. (a) Measured spectral intensity versus wavelength (μm) and laser power. (b) Fraction of laser power in each order versus incident laser power. (c) Measured (circles) and estimated (solid curve) total power efficiency.

As seen in Fig. 8(c), the total power efficiency of the Raman conversion process was directly obtained by measuring the power exiting the fiber with a thermal power meter. For increasing spectral red-shifts (or increasing powers) one finds that the total power efficiency monotonically decreases from 62% (consistent with linear losses) to 35%, indicating that nonlinearly induced power dissipation occurs at higher powers. Note that some component of the losses is a fundamental consequence of the Raman process, which requires that each Stokes-shifted photon coincides with the production of a

(dissipative) phonon. An estimate of the power efficiency attributable to Raman process (or phonon-induced losses) can be made using the known quantum efficiency of the Raman process and the measured power fraction in each Raman order, as is shown by a solid curve in Fig. 3(c), revealing reasonable agreement with measurement. The discrepancy between the estimated and measured efficiencies is most pronounced at high powers, indicating that high silica absorption losses at 2.41 μm wavelengths are limiting the efficiency of the power transfer at long wavelengths.

Finally, we examine the temporal evolution of the laser pulse through the spontaneous Raman process. The measured initial pulse profile (before entering the nonlinear fiber) is seen in Fig. 9(a), while the pulse profiles found by spectrally resolving the pump (solid curve) and first Raman order (dashed curve) exiting the nonlinear fiber can be seen in Fig. 9(b), revealing that the central portion of the pulse is transferred from 1.53 to 1.64 μm, leaving only the wings of the pulse behind. Pulse apodization of this form is well understood in the context of spontaneous Raman buildup and results from the intensity dependence of the Raman gain. These measurements agree well with temporal simulations, found through coupled amplitude equations incorporating dispersion, Kerr nonlinearities, and Raman terms, seen in Figs. 9(c) and 9(d). Interestingly, the peak pulse intensity and pulse shape are essentially preserved, allowing the same process to occur numerous times. Finally, we note that the walk-off length for the pump and Stokes wavelengths is ~300 m for 2 ns pulse durations, meaning that dispersion has little impact on the temporal evolution at these length scales.

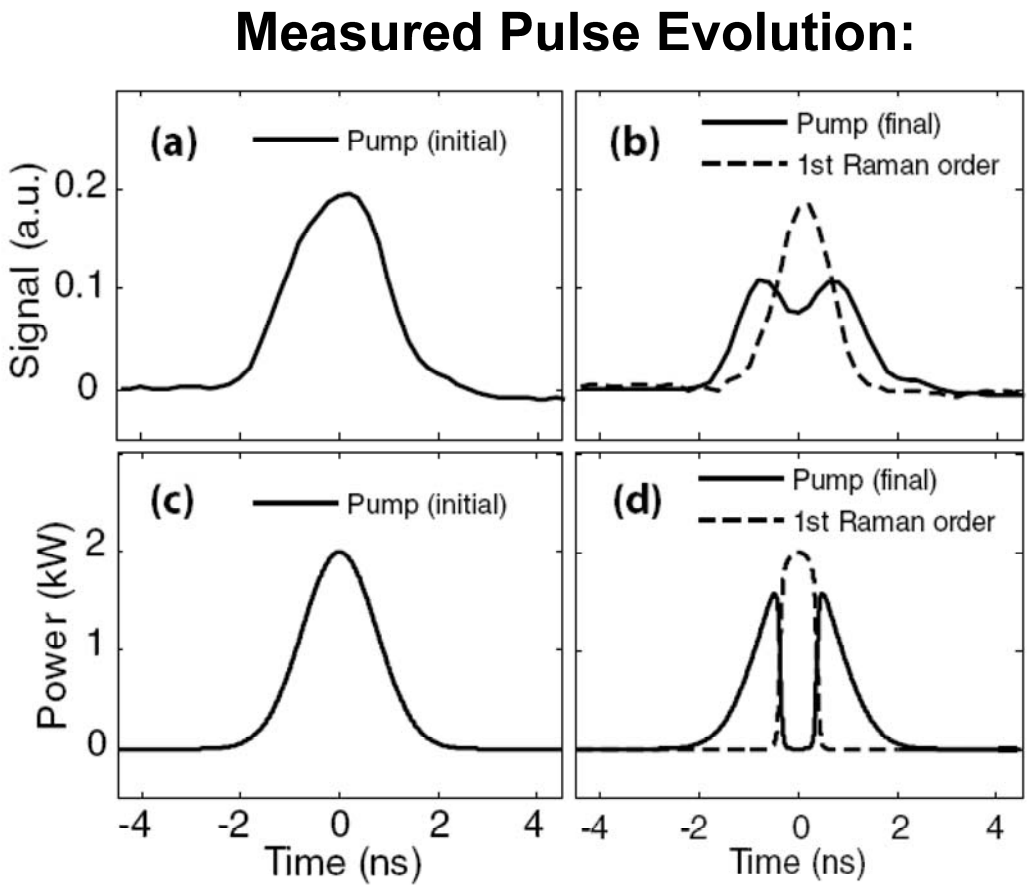

Fig. 9. (a) and (b) Measured pulse profiles. (c) and (d) Simulated pulse profiles for comparison.

In conclusion, we have shown that, through use of silica fibers possessing normal dispersion over near-IR and mid-IR wavelengths, 37% (16%) efficient Raman power transfer from 1.53 μm to 2.15 and 2.41 μm wavelength bands can be obtained using nanosecond pulses from an all-fiber laser source. In this case, the total conversion efficiencies were unnecessarily limited by fiber losses. However, efficiencies approaching 70% can, in principle, be achieved at these wavelengths if fiber losses are made negligible. Finally, in contrast to supercontinuum techniques for long-wavelength generation, we note that high levels of Raman gain generated at these wavelength bands could produce useful optical amplification necessary for the development of numerous mid-IR laser sources.

Section 2 – Fabrication of Chalco-Polymer fibers

In this section we report the fabrication of low loss chalcogenide-polymer fibers. We describe the pre-form construction process, the drawing process, and summarize the experimental characterization of the fibers yielding low optical losses over much of the MID-IR.

Section 2.1 – Fabrication of Large-core Chalco-Polymer fibers

In the following report we: (1) Describe the improved perform fabrication process and recent draw results with high purity As2Se3 glasses. (2) Report vastly improved optical performance of newly fabricated fibers through cutback measurements via laser-based and FTIR-based spectral measurements.

Through the course of this research program we have found through bulk optical transmission studies that the impurity levels were lowest with processed commercial As2Se3 glasses, leading us to expect the lowest losses with such glasses in fiber fabrication. Here we report the properties of such glasses once drawn into the form of a chalco-PES fiber. As described in previous reports, once the chalcogenide glass is cast into the form of a rod (Fig 10(a)), it is wrapped with PES polymer films (Fig. 10(b)) until a perform with the desired dimensions is achieved (Fig. 10(c)). The perform is then consolidated and drawn down by factors of 20-50 with a custom draw-tower. In this case we started with a chalcogenide rod of outer diameter 1cm and the PES outer diameter of 2.5 cm are drawn down to fibers with diameters ranging from 1600 microns to 600 microns.

Through several fiber draws, it was observed that the softening temperature was higher than those obtained through our in-house fabricated glasses, making higher bait-off temperatures necessary (312 Deg C instead of 305 Deg C). This is likely due to a difference in composition of the AMI glass. However, once the adjustments to the draw conditions were made, the draw process was stable, allowing us to draw ~100 meters of large-core chalco-PES fiber.

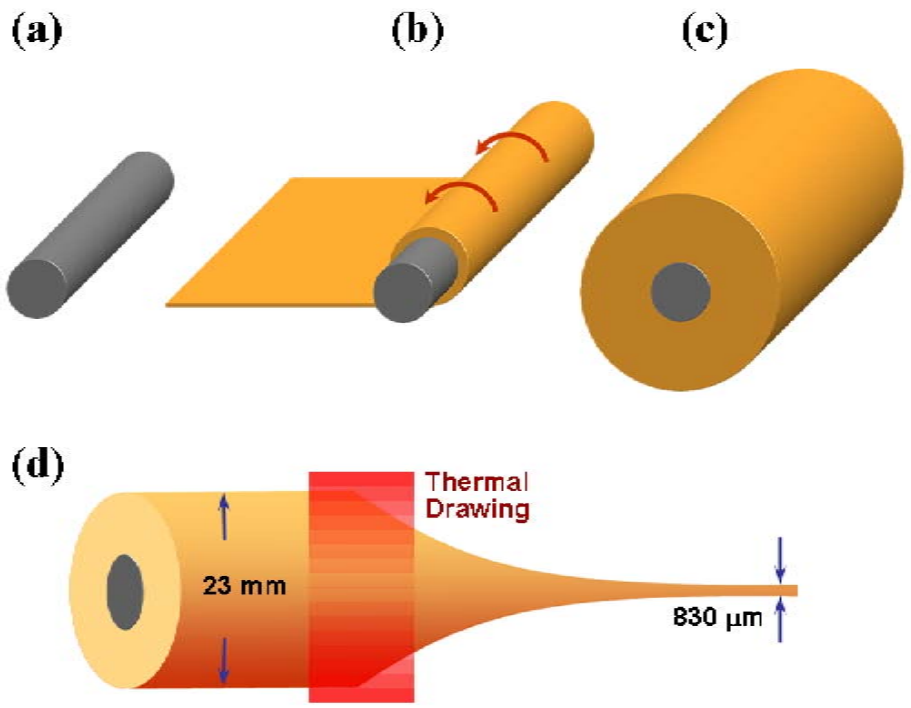

Figure 10: Schematic of perform fabrication and fiber draw. (a) shows a chalcogenide rod, onto which PES is rolled (b) until a solid chalco-PES perform is constructed (c). After consolidation, the perform is drawn into a fiber as seen in (d).

Photos of the fabricated fiber can be seen in Fig 11, along with an image of apolished fiber cross-section. Examination of a cleaved fiber cross-section reveals that the chalcogenide glass in exhibits a smooth finish, indicating that the glass quality is maintained through the fiber draw. (There doesn't appear to be a mat or textured finish, as was often found when examining the previous fibers after draw, using lower purity glasses.)

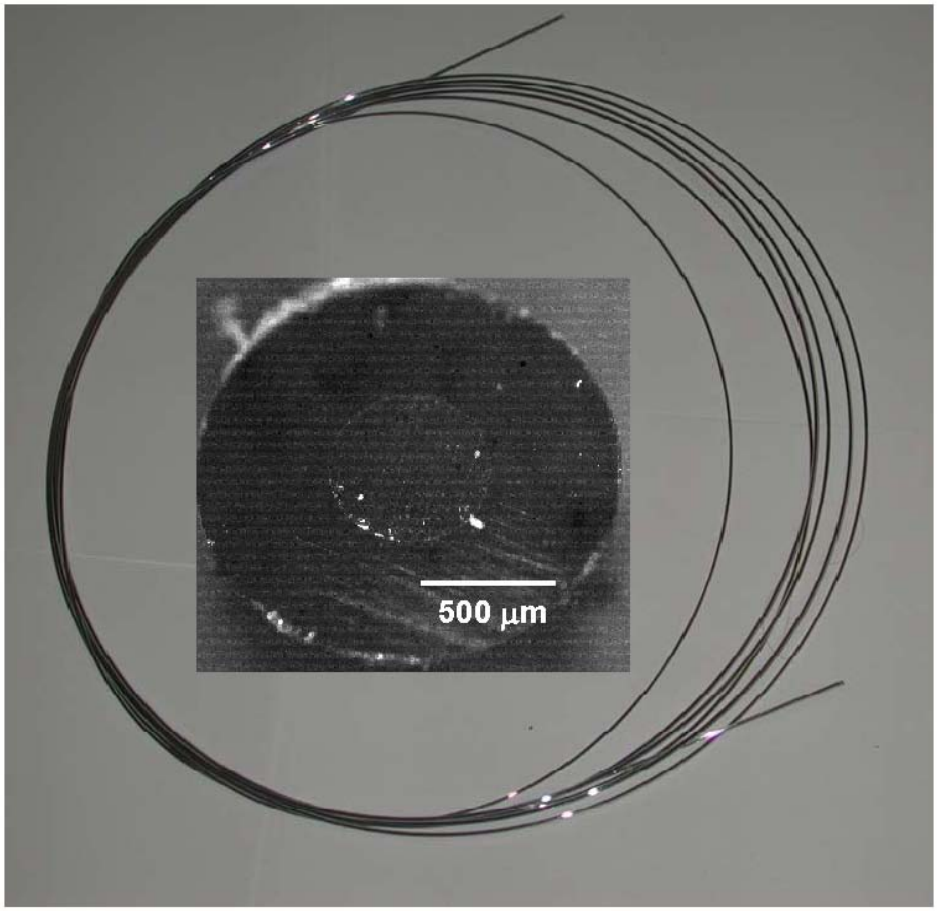

Figure 11: Photo of fabricated chaclo-PES fiber. Inset: micrograph of polished fiber cross-section.

Section 2.2– Optical properties of fabricated large-core fibers

Several lengths of these optical fibers (outer diameter 1600 microns) were polished, and cutback loss measurements were performed through various means. As will be discussed, the losses of these multi-mode fibers are estimated to be ~2dB/meter, however, as the angle of incidence of the coupled light is increased (through the use of lenses of different numerical aperture) the apparent losses increased to a value of 9db/meter. This indicates that the losses of the fiber are dominated by either (1) scattering losses at the PES-chalco interface, or (2) glass defects near that interface. From our experience with hollow core fibers (1) seems more likely at the moment.

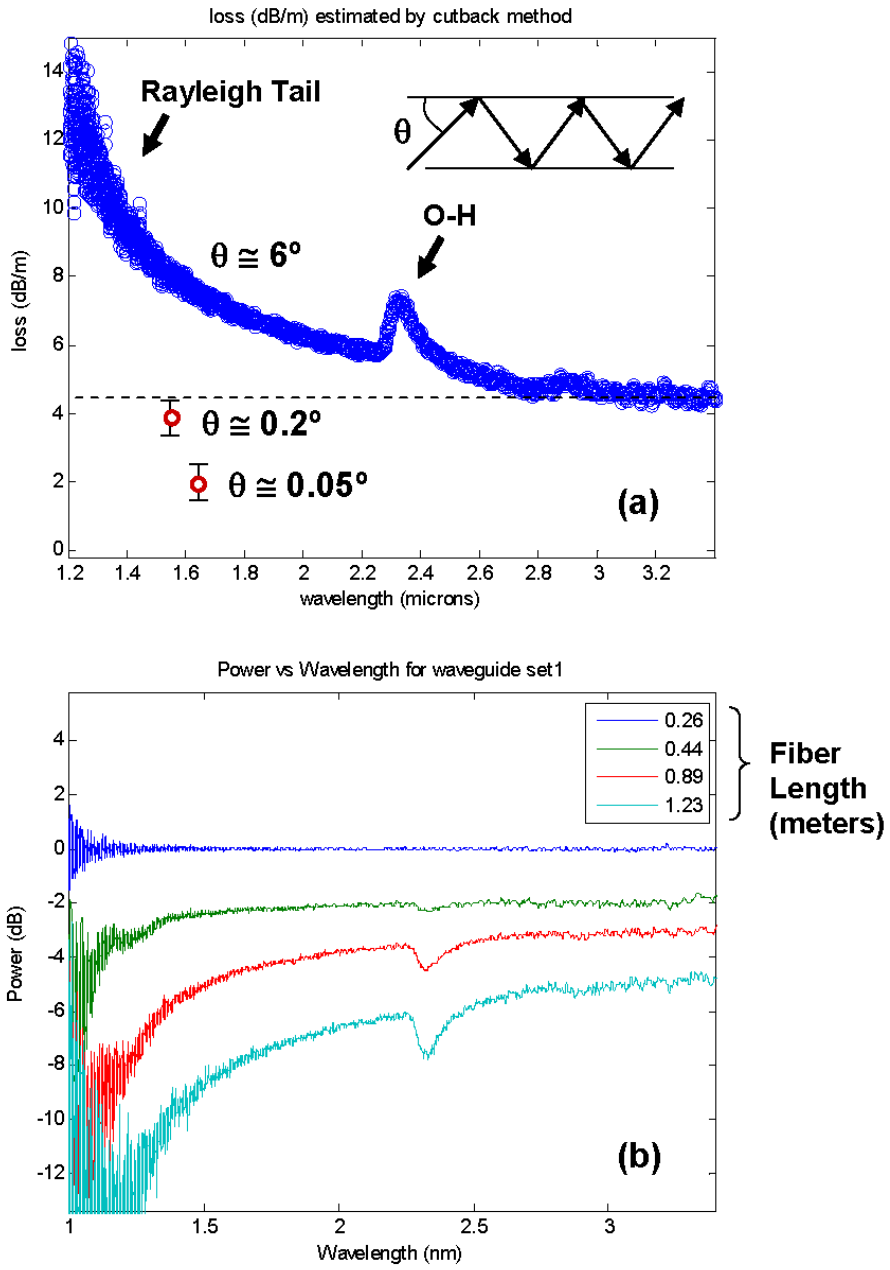

Figure 12: (a) Loss measurements obtained by cutback. FTIR measurements were obtained by processing the spectral traces seen in (b). Each blue circle is the result of a fit between three different fiber lengths. Red circles show individual measurements from laser-based cutback measurements.

Cutback measurements were performed by polishing both ends of several lengths of fiber {0.26, 0.44, 0.89, 1.23 meters), and performing transmission measurements on each fiber segment. Our first measurement of loss was performed with a narrow-band laser source at 1560 nm, and a spot size, corresponding to a maximum angle of excitation of 0.2º. These loss measurements yielded loss values of 4dB/meter. In order to better understand the loss mechanism, we also performed loss measurements through FTIR transmission. In this case the angle of excitation is estimated to be 8º, and at the same

wavelength, a loss value of 9dB/meter was found. Finally, to identify origin of the discrepancy, we performed another loss measurement on the same set of polished fibers using a 1mm diameter spot size for excitation (angle of 0.05º). This allows us to further correlate the estimated losses with the k-vector spread of the incident light. Through this measurement the lowest losses were measured, at a value of 2dB/meter. These three measurements are strong evidence indicating that the majority of the losses in our newly fabricated fibers originate from the PES-chalco interface, or from glass in the vicinity of that boundary. In fact, since we know that the axial alignment of the excitation is imperfect (as is the angle of the polish with respect to the axis of the fiber), we expect that the glass losses are even smaller than the 2dB/meter measurement would indicate.

Section 2.3– Fabrication of small core chalco-PES fibers

In the following we: (1) Describe the fabrication of low-loss small core chalco-PES fibers to 20-30 micron dimensions. (2) Characterized losses of small core chalco-PES fibers, revealing propagation losses of as low as ~6dB/meter through fiber segments ~ 0.5 meters long.

The preform fabrication process begins with a segment of large-core chalco-PES fiber, such as that seen in Fig 13(a). The fiber segment is bundled with PES fibers and rolled into a cylinder with PES films as seen in Fig. 13(c). The preform is then consolidated and drawn down by factors of 20-50 with a custom draw-tower. In this case we started with a chalcogenide fiber of core-diameter 500 microns and the PES outer diameter of 2.5 cm are drawn down to fibers with diameters ranging from 900 microns to 30 microns. The draw process is illustrated in Fig 13(d). (Note, the dimensions labeled in the illustration are irrelevant.)

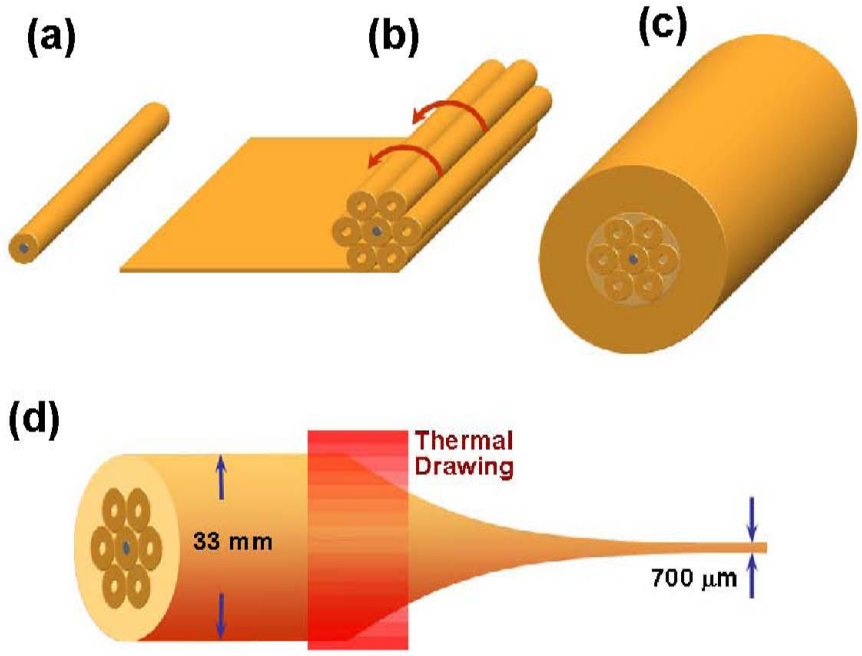

Figure 13: Schematic of perform fabrication and fiber draw. (a) Shows the large-core chalco-PES fiber which forms the center of the perform. (b) The fiber segment is stacked into a hexagonal structure with PES fibers, and then rolled into a cylinder as shown in (c). After consolidation, the perform is drawn into a fiber as seen in (d).

Section 2.4 – Loss estimates of the chalco-PES fiber

After the draw, we polished and tested 10 segments of small core fiber ranging from 15-140 cm in length in order to obtain cutback loss estimates. Through the test of these fibers, it was found that the fiber transparency of similar segments can vary a great deal. This is an indication that point defects are playing a larger role as we shrink the core size to smaller dimensions. Unfortunately, such stochastic variations in transmission properties make it difficult to nail down the fiber losses through cutback measurements. However, through careful power transmission measurements of long fiber segments, it is feasible to obtain an upper-bound on the fiber losses.

Figure 14 shows output mode from a 44cm segment of 30 micron chalco-PES fiber when excited at 1620nm with laser light. From Fig. 14(c), we clearly see that the PES cladding modes a negligible portion of the transmitted power. Through careful measurement of the incident and transmitted powers through this 44 cm segment, we find that (Transmission Losses) + (Insertion Losses) = 5.9 dB. Since insertion losses account for ~ 3dB of loss (due to Fresnel contribution alone), it is clear that the propagation losses must account for the remaining 3dB of loss. This yields an upper-bound loss figure of ~6 dB/meter for this fiber.

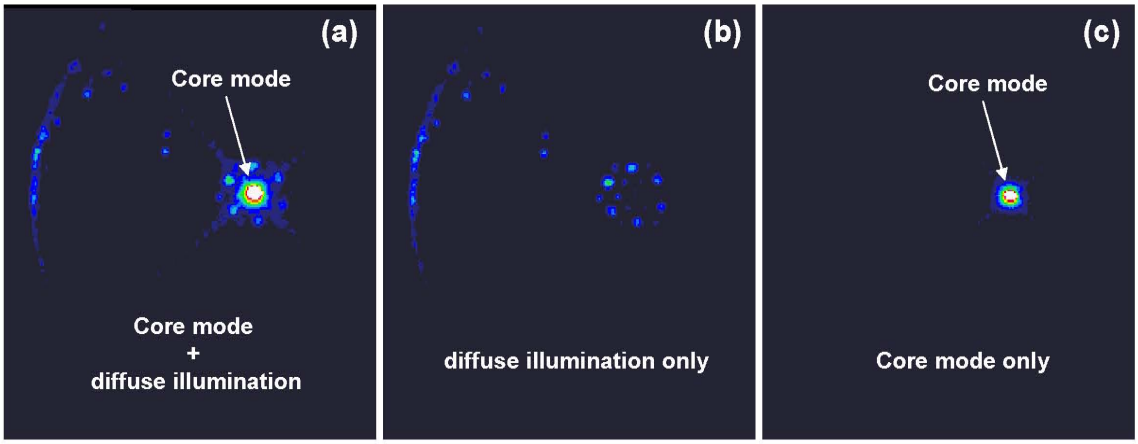

Figure 14: Photo of fabricated chaclo-PES fiber under different excitation and illumination conditions. (a) shows core-mode and diffuse illumination, allowing us to see the fiber structure and the core mode. (b) shows diffuse illumination only. (c) shows core mode excitiation.

Section 3 – Frequency-domain heterodyne reflectometry apparatus

In the following section we: (1) Describe the development of a frequency-domain heterodyne reflectometry apparatus for the quantitative study of defect densities within chalcogenide fibers. (2) We apply this apparatus to the study of losses within chalcogenide fibers.

Numerous types of defects can be detrimental to the performance of chalcogenide fibers such as: (1) bubbles formed during the cast of the glass, (2) crystalline defects within the glass, (3) dust particles within the glass or the PES, (4) cracking and breaking of the glass. Furthermore, there is always some uncertainty as to appropriate handling of the fragile chalcogenide materials. For instance, it might be possible that our polishing process induces cracks within otherwise pristine fibers, generating unnecessary losses. In order to address these issues, and better quantify the source of losses in our fibers, and the characteristic defect densities within our fibers, we have developed a highly sensitive laser-based back-scatter method.

The technique that we employ is called frequency-domain heterodyne reflectometry, which enables high spatial resolution (~20 microns) back-scatter measurements of back-scattered light in optical fibers. This measurement technique utilizes a continuously-swept tunable laser to generate a linearly chirped pulse (of millisecond duration). When this swept laser-source is used in tandem with an interferometer, of the form shown in Fig. 15, a heterodyne beat-frequency (or tone) is generated whose frequency is proportional to the difference in group-delay (Δt_g) experienced between the two arms.

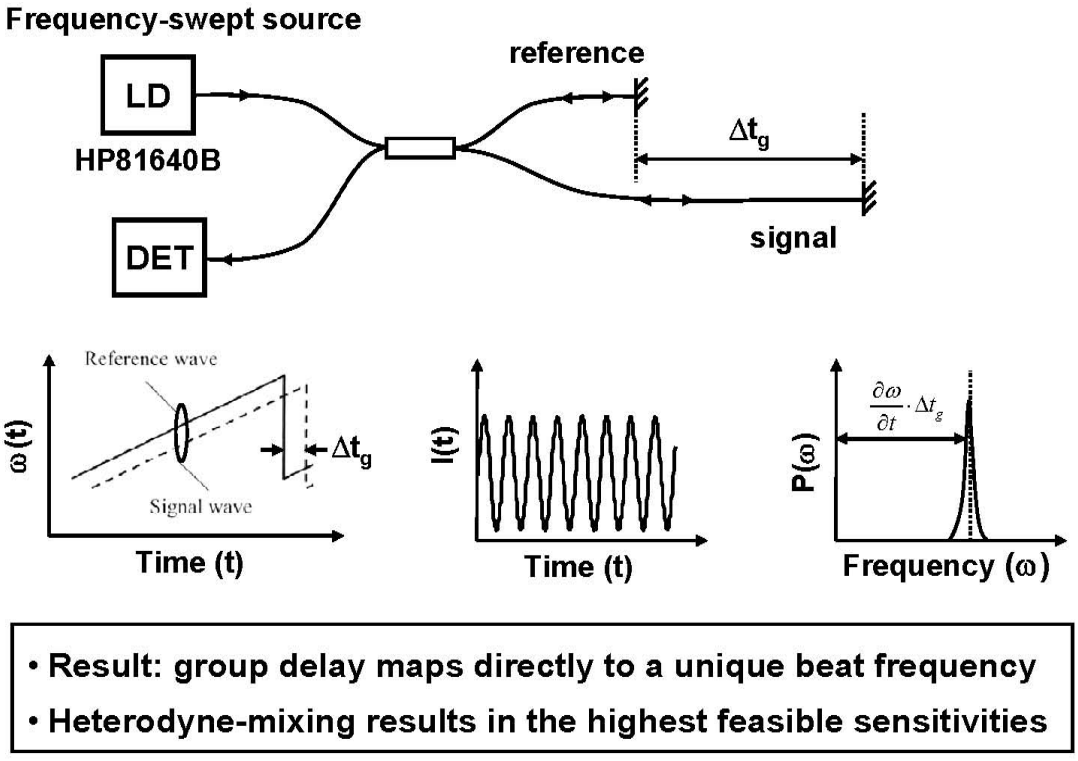

Figure 15: (Top panel) shows a simplified schematic of the back-scatter apparatus. (lower left panel) shows the frequency sweep of the reference and delayed pulses over time. (Lower middle panel) shows the heterodyne beat frequency measured by the detector whose frequency is proportional to the group delay (as seen in Lower right panel).

In reality the experimental apparatus that we have developed is much more sophisticated than that seen in Fig. 15. In reality, no tunable laser has a perfectly linear sweep with frequency. For this reason, we must use an interferometer to recalibrate the wavelength of the swept laser source. Fig. 16 shows the complete apparatus with the Fabry-Perot interferometer in the upper arm of the apparatus, while the heterodyne measurement is synchronously performed in the lower apparatus.

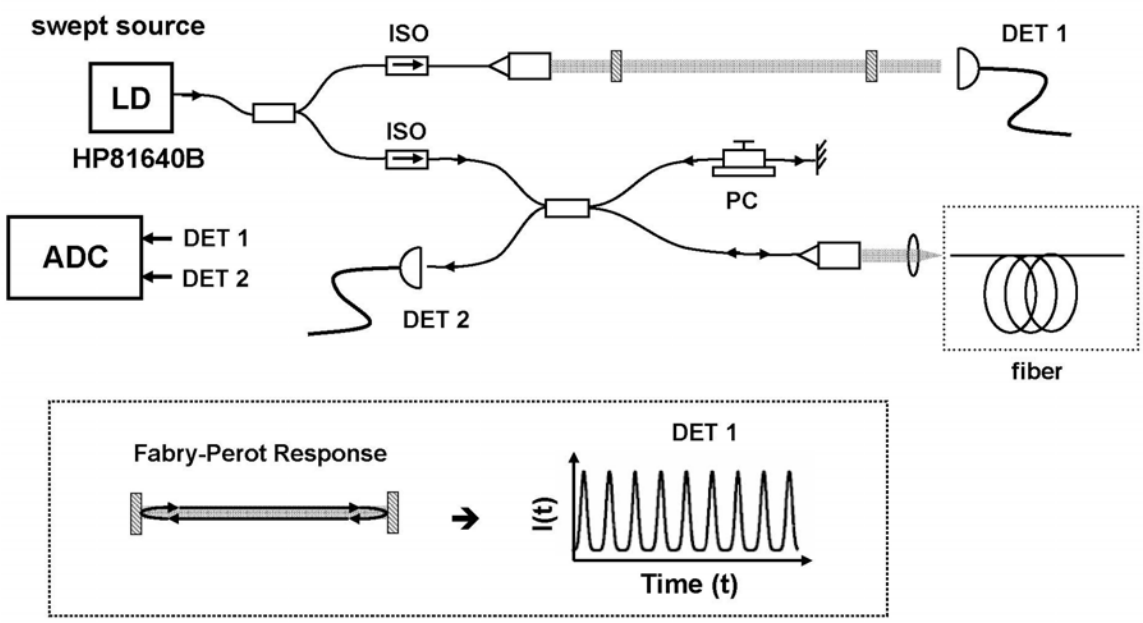

Figure 16: (Top panel) shows a complete apparatus for frequency-domain back-scatter measurement. (Bottom panel) illustrates the temporal signal obtained from the Fabry-Perot reference arm.

When this back-scatter method is applied to the study of chalcogenide fibers, we have traces of the form shown in Fig 17. The (main) top panel shows the back-scatter signal obtained through measurement of a 30 micron core chalcogenide-PES fiber. The input and output facets of the fiber are indicated with circles and labeled accordingly. Three sub-panels are shown at the bottom of the figure which are magnified views of various portions of the back-scatter data. In the lower-left we see the back-scatter signature of the fiber-optic collimator assembly, including the angle-polished fiber, and the front and back faces of the collimating lens. In the lower middle panel, we see a magnified view of numerous scattering centers within the fiber, and in the lower-right, the signature for the output facet can be seen.

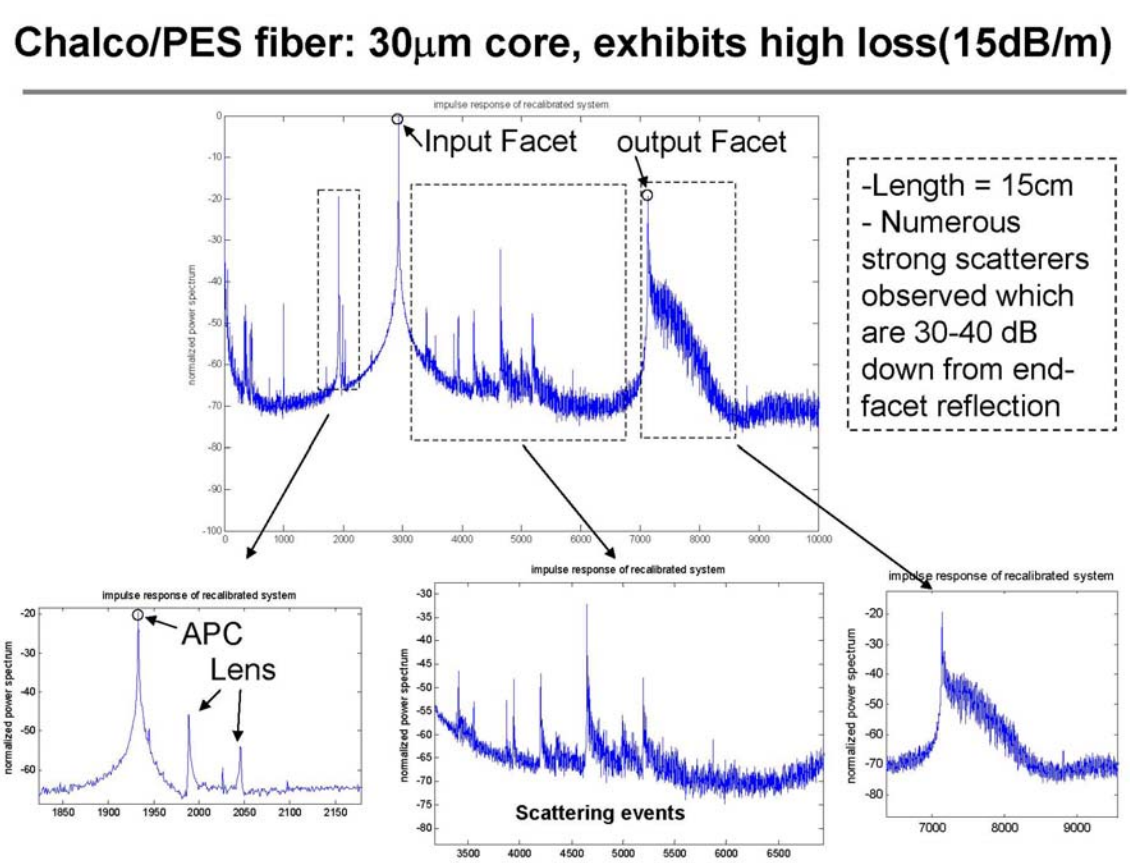

Figure 17: The back-scatter heterodyne ranging signature for a chalcogenide-PES fiber with a core dimension of ~30 microns.

Traces such as these immediately allow us to answer questions about whether handling of our fibers through polishing procedures induce cracking or damage the fibers (In fact these traces indicate that our handling of the fibers doesn't harm them, since there are no scattering signatures where we clamp the fibers). Furthermore, we can identify the density and scale of scattering defects in a fiber. In the middle section of this fiber, we clearly see several strongly scattering point defects which are very localized in space. Through the systematic study of numerous lengths of chalcogenide fiber we have found that there is generally a very high correlation between the density and strengths of scattering centers in a fiber, and the overall insertion loss that it possesses.

In conclusion, we have developed a laser-based ranging methods to quantitatively assess the size and density of defects within our chalcogenide fibers. In a short time, methods have proven to be very useful to understanding the nature of our losses. From the small scale (30-100 microns) of the scattering events that we find through the ranging method several possible defect types seem plausible (1) crystalline defects (2) micron-scale bubbles (3) morphological defects between the PES-chalcogenide materials during draw.

Section 4– Nonlinear studies of chalcogenide fibers

Detailed in the following are: (1) Observations of the onset of As_2Se_3 damage threshold with high peak power nanosecond pulses. (2) Femtosecond studies of spectral broadening in short segments of chalcogenide fiber. (3) Raman studies in longer sections of chalcogenide fibers.

Section 4.1 – Chalcogenide damage threshold

Improved surface-finish (achieved through the new polishing techniques) have greatly improved the damage threshold observed at the input facet of As_2Se_3 fibers. It was observed that devices with the highest quality optical finish yielded a damage threshold of ~5kW, while breakdown intensities of as low as 50-100W were observed in devices with a higher degree of surface roughness. The results of laser damage can be seen through the optical micrographs of Fig.18.

Since damage threshold poses a fundamental limitation for chalcogenides as nonlinear materials, this issue warrants a great deal of attention. As we know, damage threshold at material interfaces can be impacted by numerous factors, the most obvious of which are:

1. Particles & surface contaminants
2. Material refractive-index
3. Interface quality (i.e. surface roughness)

Though, it is primarily due to factors (1) and (3) that materials (and fibers) virtually always exhibit a lower damage threshold at material interfaces. It is clear that particles

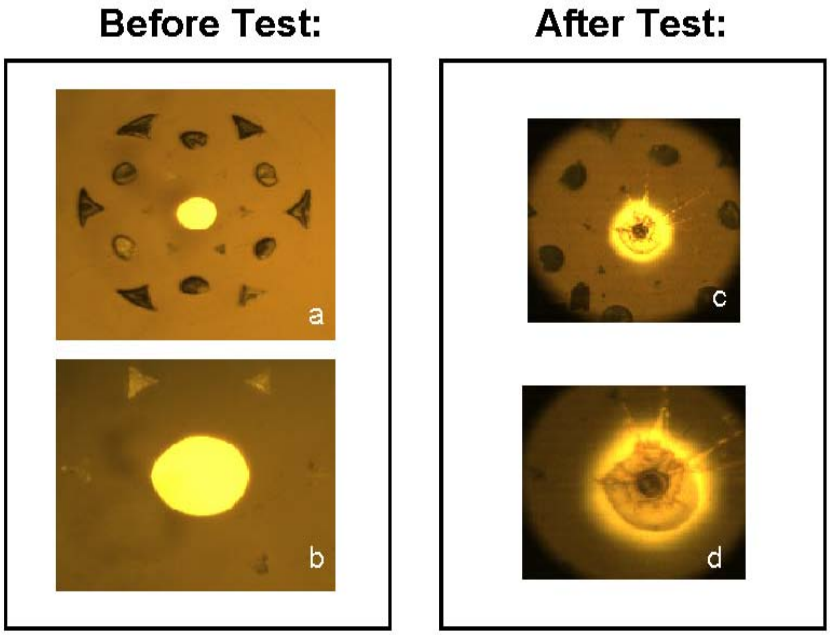

Figure 18 Optical micrographs of step-index chalcogenide fiber before and after studies with high-power nanosecond pulses. (a) & (b) show the polished chalcogenide core (gold circle) before test. (c) & (d) show a similar fiber after test at peak powers of several kilowatts of peak power. A crater-like oblation of ~10 μm dimensions can be seen in the center of the fiber.

and contaminants can seed breakdown through thermal runaway. However, surface contaminants also contribute field distortions, which are the primary problem caused by surface roughness (i.e. no (3)). Field distortions are not only problematic for achieving high coupling efficiencies into single mode fibers, but they also result in field-enhancements within the material, which artificially reduce the damage threshold of a material.

As a trivial example, one can imagine a plane-wave traversing a highly textured interface, thereby incurring random phase variations. As the beam propagates, these phase variations will express themselves as intensity variations (or hot-spots) on the propagating beam. For a given surface topography, the phase variation acquired will clearly depend strongly in the refractive index of the material. Though, it is worth pointing out that this is a gross simplification of the behavior at an interface. In reality, the field-enhancement at the surface is significantly more complicated, since it involves near-field effects (which are also highly dependent on material refractive-index) resulting in local field enhancements at the interface between chalcogenide and air. In fact, the high refractive index (n = 2.8) of the chalcogenide materials may significantly increase the local field enhancement (in comparison to silica counterpart), warranting a computational study. So far, we have observed a significant improvement in the damage threshold due to an improvement in surface quality, though, before more effort is invested in the surface preparation, a short computational study could shed light on the impact it could have.

Finally, it is interesting to comment on the nature of the material breakdown observed in Fig.1. In most instances observed in the laboratory, thermal runaway results in the collapse of the polymer structure, leaving little to see. However, in this case, experiments were stopped as soon as a change in optical performance of the fiber was observed, leaving us some evidence of the breakdown mechanism. Fig.1 reveals a distinct "crater" which is approximately the same dimension as the 10μm fiber-mode used for excitation. Furthermore, molten chalcogenide is projected on the surface of the fiber, indicating a rapid vaporization of the chalcogenide has taken place. Presumably, this vaporization results from the change in temperature generated by a single nanosecond pulse. From these images, the laser parameters (i.e. repetition rate, pulse energy, pulse duration) and from the material parameters (thermal conductivity, heat capacity, linear and nonlinear absorption and carrier density –N(T)-), we have enough information to begin constructing a simple model of the As_2Se_3 breakdown mechanism. This is important, since it will allow us to determine the pulse regime that will yield the highest peak power before inducing breakdown.

Section 4.2 – Femtosecond Nonlinear optical studies of chalcogenide Fiber

Optical studies of the fiber array were carried out with the apparatus seen in Fig. 19. High peak intensity 150 femtosecond pulses are coupled into the fiber core with a free-space microscope objective. The transmitted optical mode is imaged with an InGaAs camera and spectrally analyzed with an optical spectrum analyzer (OSA). See Fig. 19 for specifics.

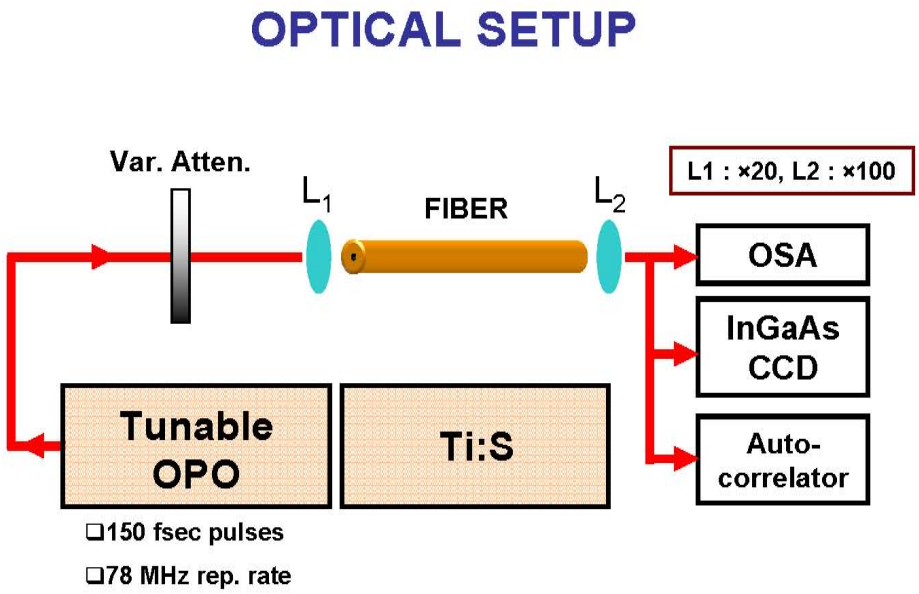

Figure 19: Optical measurement setup used for nonlinear studies of chalcogenide fibers.

As the nonlinear fiber is optimally coupled, with a launch power of 160 mW, a drastic broadening of the spectrum is observed. As can be seen in Fig. 20, the incident laser pulses, of bandwidth 20 nm is broadened to ~200 nm after self-phase modulation (SPM) occurs in the fiber segment. In these experiments, a one centimeter fiber segment was used. The fiber device was prepared through the methods described in section 2.

These SPM results are very promising considering that the fiber exhibits a large normal dispersion (magnitude ~ 600ps/nm-km). At longer wavelengths the magnitude of dispersion is much lower, which should enable a more drastic spectral broadening.

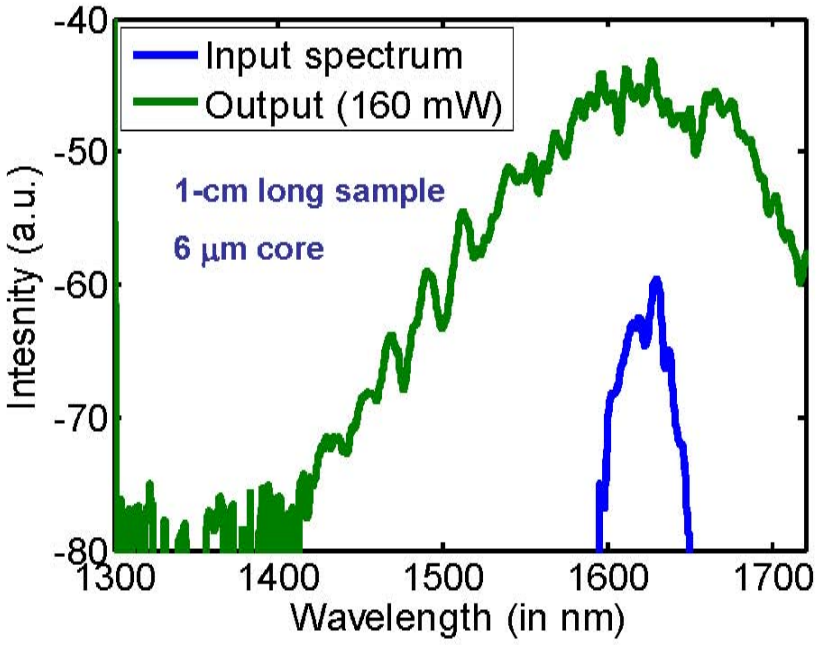

Figure 20: Laser spectrum before (blue) and after (green) transmission through a chalcogenide fiber having a 6 micron core.

In all, these measurements allow us to estimate the nonlinear properties of our chalcogenide materials, and determine the peak powers that the fiber can sustain through use of femtosecond pulses. Unfortunately, femtosecond based supercontinuum generation doesn't provide a practical path to practical mid-IR generation in chalcogenide fibers, as femtosecond sources are not readily available in the mid-IR.

It should also be noted that through these measurements, the degree of spectral broadening seen above was rather short lived due to an instability of the chalcogenide fiber when exposed to such high peak powers. We suspect that free carriers were being generated through multi-photon processes, resulting in plasma-optic induced dissipation of optical power within the fiber. After a few minutes of high power exposure, we often observed a change of spectral shape of the supercontinuum corresponding to an abrupt drop in bandwidth. Such spectral instabilities might be explainable by thermally induced modal instabilities (resulting from plasma-optic absorption).

Section 4.3 – Cascaded Raman Amplification in Chalcogenide fibers

Here we examine the Raman gain of the chalcogenide fiber through excitation of the 30 micron core chalco-PES fiber with high peak-power nanosecond pulses. The laser source used is shown schematically in Fig. 21. It consists of a DFB laser (1531nm center wavelength) which is driven by a pulse generator to produce ~1ns pulses. These pulses are then amplified to 1-2 kW peak powers with three stages of amplification. Propagation through short segments of silica SMF which precedes the chalcogenide fiber device results in Raman transfer of the peak power of the pulse to the adjacent Raman order (i.e. red-shifting by~13THz). This results in approximately half of the optical power at 1530 nm and half at 1640 nm. Though it is important to note that the pulses

transferred to the 1640nm wavelengths are of much higher peak power due to the nonlinear nature of the Raman process.

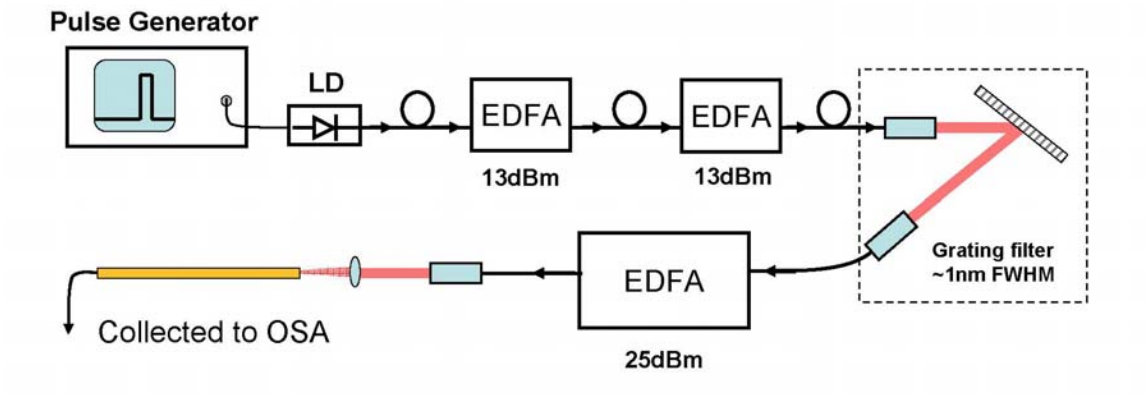

Figure 21. A schematic of the nanosecond fiber-laser source used for excitation of chalcogenide fibers under study.

To clarify this process, we show the theoretical pulse evolution for a 2kW peak power pulse in a silica fiber in Fig. 22. We see that the central portion of the pulse (i.e. the portion of the pulse which is of highest peak power) is transferred to the Stokes frequency, while the wings of the pulse are left behind. This behavior was verified through temporal measurements of the pulse shapes generated by the laser at the two different wavelengths generated at the output of the laser. The spectral output of the laser can be seen in Fig. 23a, revealing that approximately half of the laser power is at 1530 nm while the other half is transferred to 1640nms. To better estimate the peak intensities produced at both wavelengths, we spectrally filtered the light seen at each wavelength and performed temporal measurements with a high speed detector. Fig 23b reveals that as the amplifier power is increased, the pulses develop a null at their center, while, Fig 23c shows a narrow pulse of increasing amplitude (with increasing amplifier power). These traces are consistent with the temporal evolution expected through simulations, revealing that the highest intensity portion of the pulse (i.e. the peak) is red-shifted to the Stokes frequency through interaction with the silica fiber.

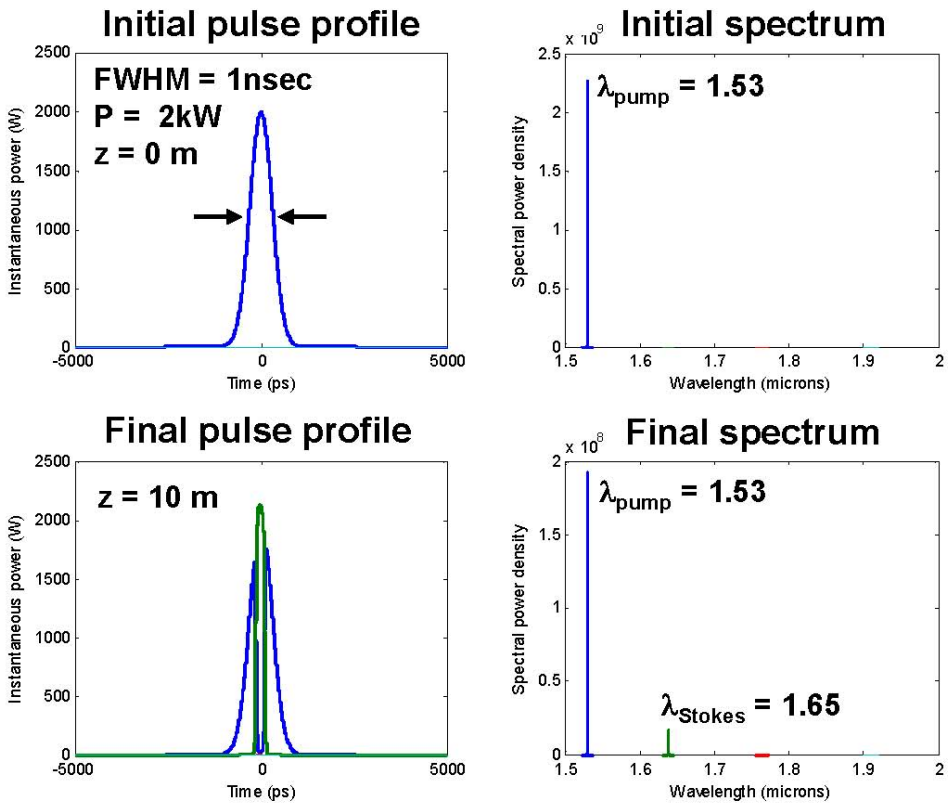

- The peak of the pulse is transferred to adjacent order
- Wings of pulse remain behind
- Results in pulse shortening!

Figure 22: Theoretical evolution of a 1ns pulse in a silica fiber. Top two panels show the temporal and spectral content of the pulse, while the bottom two panels show the temporal and spectral content after propagation of ~10meters of silica SMF 28

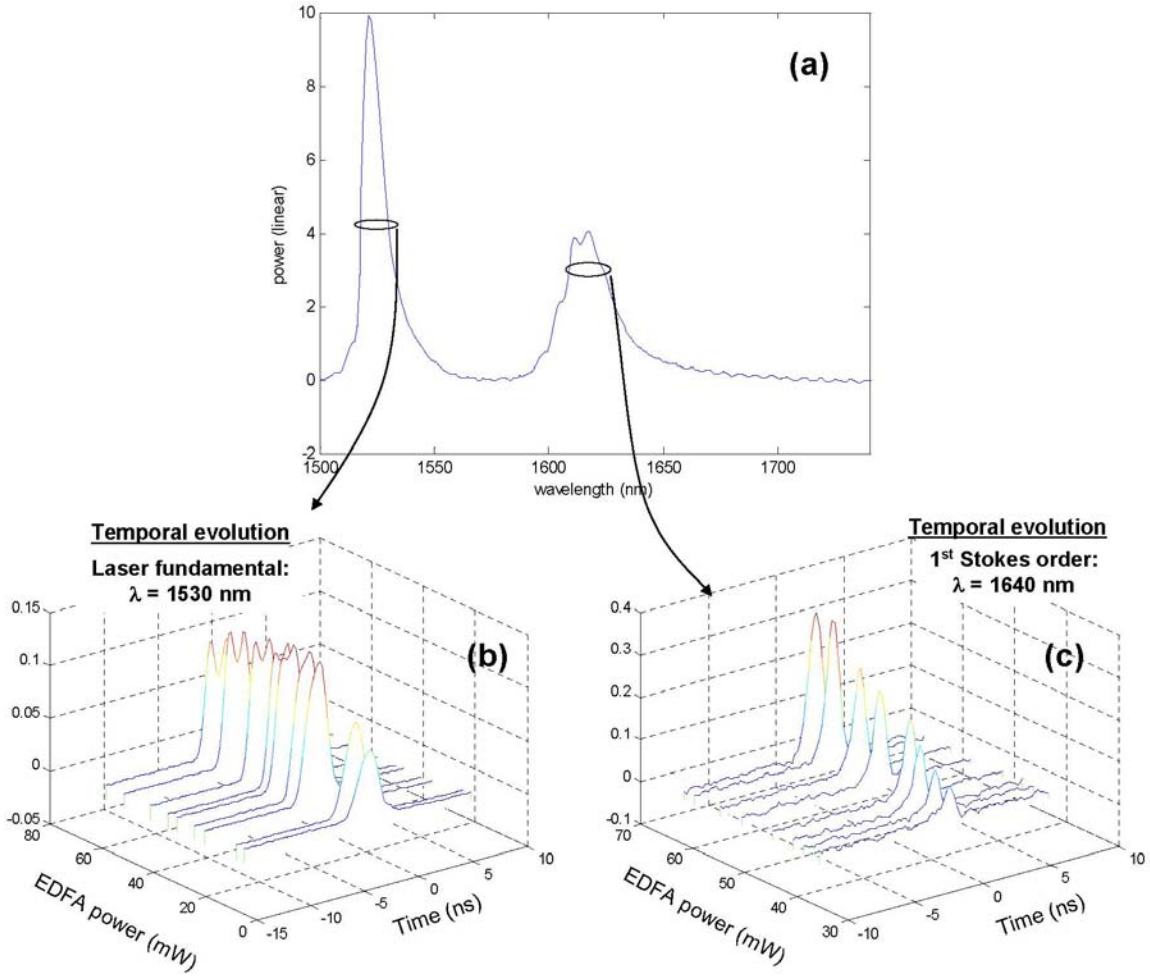

Figure 23: (a) Measured spectrum at output of fiber-laser revealing optical power at both 1530 nm and 1640 nms. (b) Temporal measurement of the 1530nm pulses and (c) 1640 nm pulses.

Pulses from the laser (i.e. of the form shown above) were coupled into a 45 cm segment of 30 micron As2Se3 fiber (described in last report) exhibiting ~6dB/m losses. Coupling into the fiber was achieved with aspheric lenses, and the spectrum emanating from the fiber was collected by butt-coupling with a silica SMF fiber. The collected spectrum was then measured with an optical spectrum analyzer (OSA). Two separate measurements obtained at different powers can be seen in Fig 24.

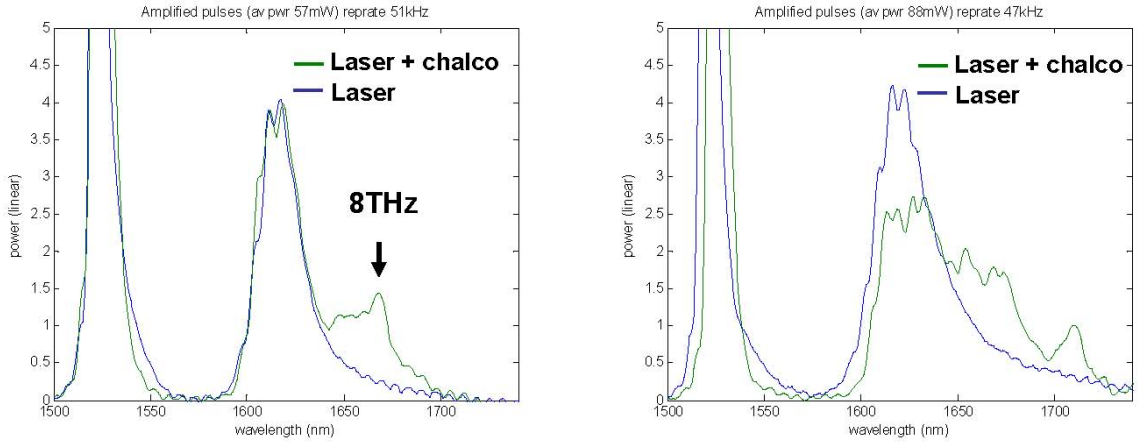

Figure 24: Left panel shows the input laser spectrum (blue) and the laser spectrum at the output of the chalco fiber (green) for ~1.5 kW peak power, while the Right panel shows the same measurement for ~2kW peak powers.

As seen in Fig. 24, the chalcogenide fiber produces a spectral red-shift of increasing magnitude for increasing laser powers. For a pulse peak power of ~1.5 kW, an 8THz frequency shift is observed which is consistent with the Raman shift of As2Se3. As the pulse peak power is increased to 2kW, further red-shifting is observed. With further increased in the laser power levels, the fiber end-facet was destroyed. Since higher damage-thresholds have been observed, we suspect that this was likely due to: (1) drift of coupling to the core of the fiber, (2) texture on the endfacet (i.e. inadequate polishing), and (3) laser power fluctuations. All of these will be investigated and improved upon in order to extend the damage threshold further.

Although there is a notable power transfer to the Stokes frequency, the Raman gain produced by the fiber is not apt to be sufficient to produce cascaded Raman from spontaneous emission. It is more likely that small amounts of laser emission are seeding the amplification process within the chalcogenide fiber. Nevertheless, this was a useful nonlinear experiment, allowing us to assess the nonlinear performance of the materials system, study the damage threshold of our chalcogenide materials, and fibers.

Section 4.4 – Further Comments on the Prospect of Cascaded Raman Amplification in Chalcogenide Fibers for Mid-IR Generation.

The primary barriers that we must overcome in order to achieve efficient chalcogenide-based cascaded Raman amplification extending our spectral reach within the MID-IR are: (1) The development of single-mode chalcogenide fibers with lower losses, enabling longer interaction lengths, (2) Mitigation of laser-induced damage of the chalcogenide fibers.

The development of low loss highly nonlinear chalcogenide fibers requires more sustained materials science studies of the glass quality before and after the fiber drawing process, possibly over a 1-2 year time frame. Due to the complex nature of the laser induced breakdown of chalcogenide glasses, there are likely a number of factors at play. However, through nonlinear studies of the fibers we have fabricated, we have discovered that, when the laser excitation is spectrally narrow, laser-induced gratings are formed

within our fibers. Such gratings likely result from spatially dependent trapping of free carriers produced by standing waves (formed by reflections from the fiber end-facets). In many cases, the induced gratings were so pronounced that the incident laser light is completely back-reflected. Of course, such back reflections are very problematic, as they severely limit the nonlinear interaction length that can be achieved.

One way to mitigate the formation of such gratings is to ensure the nanosecond laser excitation in use is spectrally broad. However, the caveat is that the laser pulses must not have spurious spikes in power (as is often the case from multi-mode laser cavities such as that of an Nd:YAG).

Conclusions

The goal of this program was to develop a multi-watt mid-IR laser source spanning the 2-5 micron wavelength range with a multi-watt output. The primary challenges faced in meeting these goals were: (1) to develop novel multi-material chalcogenide optical fibers to facilitate nonlinear spectral generation over the 2-5 micron wavelength range, (2) to engineer and validate a novel laser source (based on nonlinear processes) which could enable the generation of 2-5 micron wavelengths within such chalcogenide materials systems, (3) implement the novel laser source concept using chalcogenide fibers and scale to high powers.

Through the life of this program, we have made tremendous strides in the development small-core, highly-nonlinear chalcogenide fibers in hybrid chalcogenide and polymer materials systems, and we were successful in developing and demonstrating a novel type of cascaded Raman laser which operates optimally in normal dispersion (a critical requirement for efficient spectral generation in chalcogenide fibers). Through validation of our new laser concept we demonstrated highly efficient transfer of power from 1.5 microns to 2.41 microns in normal dispersion silica fibers. Furthermore, we have performed extensive nonlinear studies on our newly developed chalcogenide fibers at both nanosecond and femtosceond timescales, demonstrating spectral generation through both stimulated Raman spectral generation and self-phase modulation. However, due to the complicated nature of chalcogenide materials system, further work is required before we can meet the challenging goals of the program. Currently there are two primary challenges that require further work: (1) Further work must be done to understand the various mechanisms for damage of chalcogenide fibers. (2) Further work is required to reduce the losses of our fibers and improve the purity of the chalcogenide materials used. Through nonlinear studies, we have found that optically induced damage to the fibers was observed at a wide range of powers (often much lower that expected), indicating that we are not currently limited by the fundamental material damage thresholds. Currently, laser-induced damage and the limited interaction lengths achieved through our fibers limit our ability to extend the spectral output of our laser system using our newly developed chalcogenide fibers.